Recovery of spatial frequencies in coherent diffraction imaging in the presence of a central obscuration

Atoosa Dejkameh[a,b], Ricarda Nebling[a,b], Uldis Locans[b], Hyun-Su Kim[b], Iacopo Mochi[b], Yasin Ekinci[b]

[a]*ETH Zürich, Rämistrasse 101, Zürich, 8092, Switzerland*
[b]*Paul Scherrer Institute (PSI), Forschungsstrasse 111, Villigen, 5232, Switzerland*

Abstract

Coherent diffraction imaging (CDI) and its scanning version, ptychography, are lensless imaging approaches used to iteratively retrieve a sample's complex scattering amplitude from its measured diffraction patterns. These imaging methods are most useful in extreme ultraviolet (EUV) and X-ray regions of the electromagnetic spectrum, where efficient imaging optics are difficult to manufacture. CDI relies on high signal-to-noise ratio diffraction data to recover the phase, but increasing the flux can cause saturation effects on the detector. A conventional solution to this problem is to place a beam stop in front of the detector. The pixel masking method is a common solution to the problem of missing frequencies due to a beam stop. This paper describes the information redundancy in the recorded data set and expands on how the reconstruction algorithm can exploit this redundancy to estimate the missing frequencies. Thereafter, we modify the size of the beam stop in experimental and simulation data to assess the impact of the missing frequencies, investigate the extent to which the lost portion of the diffraction spectrum can be recovered, and quantify the effect of the beam stop on the image quality. The experimental findings and simulations conducted for EUV imaging demonstrate that when using a beam stop, the numerical aperture of the condenser is a crucial factor in the recovery of lost frequencies. Our thorough investigation of the reconstructed images provides information on the overall quality of reconstruction and highlights the vulnerable frequencies if the beam stop size is larger than the extent of the illumination NA. The outcome of this study can be applied to other sources of frequency loss, and it will contribute to the improvement of experiments and reconstruction algorithms in CDI.

Keywords: Ptychography, CDI, Diffraction, EUV, Lensless imaging

1. Introduction

Ptychography [1, 2, 3] is a scanning coherent diffraction imaging (CDI) technique that has gained significant popularity in the last decade. In this method, the sample is locally illuminated by a coherent probe, and a series of diffraction intensity patterns from overlapping locations on the sample are collected.These diffraction patterns are then processed using a phase retrieval algorithm to reconstruct the object's complex amplitude, which provides a detailed image of the sample. Ptychography has a broad range of applications from the imaging of nanostructures [4, 6] to the investigation of biological samples [7] and three-dimensional objects [8] including integrated circuits [9]. While its application areas are diverse, ptychography is often used in the spectral range from extreme ultraviolet (EUV) to hard X-Rays, where efficient optical elements are challenging to manufacture. At EUV wavelengths, for instance, the high absorbance of most materials makes it impractical to work with refractive optics, and therefore, imaging systems rely mostly on diffractive optics, such as Fresnel zoneplates or multilayer-coated mirror. However, Fresnel zoneplates often have limited efficiency, and reflective EUV optics is wavelength-specific and difficult to manufacture particularly with high numerical aperture (NA)[10, 11].
Ptychography replaces the functionality of the imaging optics with a computational approach that yields aberration-free images of the object's complex scattering amplitude. Reconstruction quality depends heavily on the quality of the measured diffraction patterns [12], which can degrade due to a variety of noise sources, including shot noise, thermal noise, readout noise from the CCD, and defects on the detector caused by cosmic radiation or dead pixels [13]. The high frequencies on the detector are often weak, but they are of particular importance since they determine the resolution limit of the reconstructed image. To improve the signal-to-noise ratio, either the intensity of the illumination or the acquisition time can be increased. As the number of photons on the detector is increased above a certain level, due to the camera's limited well depth, the oversaturated pixels start to spill to the neighbouring pixels and create a bleeding effect, as shown in Fig. 1. While the intensity range of the diffraction pattern depends on the sample structure, in most cases, the central area of the diffraction pattern has the highest intensity and is the first to saturate the detector. A practical solution to this problem is using a beam stop that blocks the most intense part of the diffraction signal, allowing the detection of the high frequencies without risking the saturation of the camera pixels. The drawback of using a beam stop is losing information in the low-frequency range. Methods that have been developed over the years to address this issue are

replacing the missing frequencies with data calculated from a low resolution image [14, 15], using a semi-transparent beam stop [16], or by employing compressed sensing methods if the object can be considered to be sparse [17].

The pixel masking method consists of instructing the reconstruction algorithm not to apply the Fourier constraint to the area with missing data [18]. This method is commonly used to recover the frequencies lost because of the beam stop [19, 20, 21, 22]. Miao et al. [23] have addressed the problem of missing information due to a beam stop in a coherent diffraction microscopy setup and concluded that, as long as the missing data is limited to the center speckle and there is sufficient oversampling, the lower frequency components masked by the beam stop can be recovered. The paper states that the number of the missing speckles, characterized as the ratio of missing pixels to the oversampling ratio, is a critical factor in predicting the quality of recovery. We expand on this topic by providing a proof of the relation between the numerical aperture of the illumination and the maximum size of the beam stop which allows a complete reconstruction. We show that for systems with a larger numerical aperture, the information is distributed over a wider angular range and can be used by the recovery algorithm.

The theoretical discussion that we present in this paper agrees with the ground work described by Pan et al. [24]. They investigate the formulation of CDI to discuss the impact of the convolution of object by the probe on the ability of CDI to recover the missing information due to saturated pixels. They investigated the effect of saturated pixels as a source of frequency data loss for plane-wave illumination in CDI. Liu et al. [25] found out that when using a plane wave illumination, ptychography is generally more tolerant to the size of the beam stop than other CDI methods . [26] finds a relation between the critical percentage of random missing frequency intensity information and the oversampling ratio of the system. This research mentions the crucial role of the spatial positions of the missing frequencies in the reconstruction procedure. It specifies that the before-mentioned relation would no longer hold for the missing central frequencies, and even a few missing central frequencies can prevent the recovery procedure from converging. In this research, we show how the illumination NA impacts the affordable number of missing central frequencies and provide a theoretical explanation of this phenomenon.

Specifically, we investigate the extent to which we can use the pixel masking method for low frequency information retrieval in the presence of a beam stop. We trace the reconstruction algorithm and show how a Fourier magnitude projection based algorithm and a finite illumination NA go hand in hand to enable the recovery of the missing frequencies. The problem of information loss due to a beam stop,

gaps between the modules of a tiled detector, or defect pixels is common in the short wavelength CDI community. Therefore, the perspective and deeper insight provided in this paper can help future research on deciding the optimal size of the beam stop and opens new possibilities for using the pixel masking method for other sources of data-loss. Section 2.1 addresses how the finite NA illumination encodes the object spectrum in an extended region in the Fourier plane. Then, we show analytically how the iterative algorithm gains access to the missing frequencies through the knowledge of the illumination. The experimental and simulation results in Sections 3.1 and 3.2 demonstrate the crucial role of illumination NA for the information loss in the Fourier domain and provide evidence on the critical size of the beam stop.

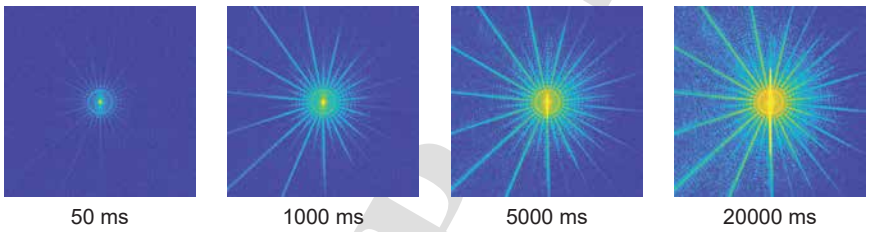

Figure 1: Bleeding effect for different exposure times due to the limited well depth of the CCD. With increased exposure time, the signal to noise ratio in the high frequency regions of the spectrum improves. On the other hand, the risk of over-saturation of the CCD pixels increases correspondingly.

2. Method

When using a beam stop, the central part of the diffraction pattern on the detector is lost. The following analytical explanation and the experimental evidence we present in Section 3.1 show that, as long as the spectral components blocked by the beam stop are also encoded in the unobstructed regions of the diffraction pattern, the image reconstruction algorithm can access the missing frequencies. We link the availability of the spectral information to the illumination NA and we prove that the critical size of the beam stop is directly related to the illumination profile.

In the following, we first establish the redundancy of frequency information in the spectra collected by the camera. Then, we show how the reconstruction algorithm can access the available valid information to fill the missing sections.

2.1. Information encoding with finite NA illumination

For a thin object, the exit wave is the product of the illumination and the object [32]. Let $o(x)$ be the object transmission function and $p(x)$ the illumination function. The exit wave directly after the object is defined as:

$$\psi(x) = o(x) \cdot p(x) \tag{1}$$

A probe with a finite numerical aperture (NA_{ill}) can be considered as a continuous distribution of tilted plane waves with propagation angles within $[-\alpha, +\alpha]$. In the following, instead of considering the whole range of the plane waves, we consider a simple 1-D case where the illumination function $p(x)$ is constituted by two mutually coherent plane waves propagating from opposite angles $\pm\alpha$:

$$p(x) = \exp(i\alpha x) + \exp(-i\alpha x) \tag{2}$$

Applying the convolution theorem, we can argue that the Fourier plane spectrum is the convolution of the object and probe spectra. Bearing in mind that the Fourier transform of a tilted plane wave is a shifted delta function, the far-field spectrum becomes,

$$\begin{aligned} \Psi(u) &= \mathrm{FT}[o(x)] * \mathrm{FT}[p(x)] \\ &= O(u) * (\delta(u-\theta)) + \delta(u+\theta)) \\ &= O(u-\theta) + O(u+\theta) \end{aligned} \tag{3}$$

Eq.3 demonstrates that for a probe composed of two plane waves, the object's spectrum is available at two locations in the far-field.

As seen in Fig. 2(b), the diffraction spectrum shifts on the detector plane when the illumination angle changes. The maximum extent of the shift and, thus, the width of the diffraction spectrum depends on the extent of the illumination NA. Fig. 2(c) illustrates the diffraction pattern produced by a finite NA illumination from summation of diffraction spectra propagating from the sample at different angles.

Fig. 3 depicts four diffraction patterns of a grating object when illuminated with different illumination NAs. The diffraction orders are non-overlapping for the smallest illumination NA of 0.023, Fig. 3(a). For larger illumination NAs, the diffraction orders do not change position but become wider. Therefore, the frequency information for each order is distributed over a larger area. This is due to the object being illuminated from a broader range of angles. The ±2 diffraction orders are outside the detector area (red square) for the smallest NA, but an increasingly larger portion of them gets inside the detector as the illumination NA increases.

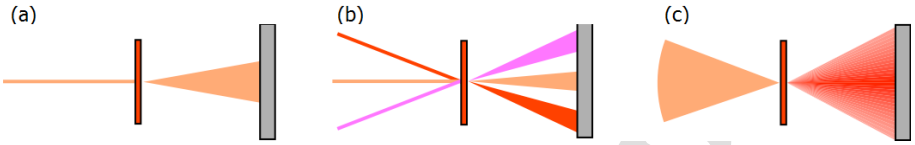

Figure 2: Comparison of the unidirectional illumination and the finite NA illumination. (a) A plane wave is illuminating the sample, producing the diffraction pattern on the detector plane. (b) If several plane waves are used, then the resulting pattern on the observation plane is the sum of all the diffraction spectra. (c) The pattern produced by an illumination with a finite NA.

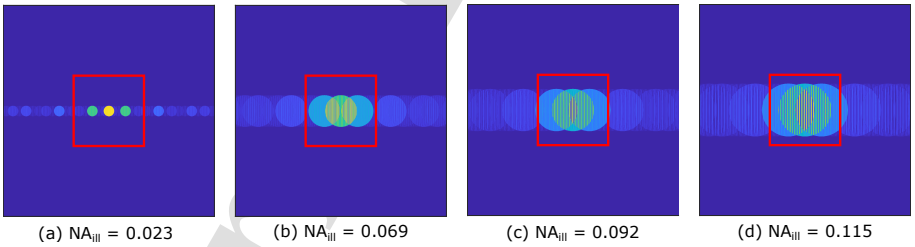

Figure 3: Diffraction patterns of a grating object when illuminated with different illumination NAs. The red rectangle represents the detector area. For larger illumination NAs, the frequency information is distributed over a larger area.

2.2. Missing frequency information retrieval in CDI

There is a large class of image reconstruction algorithms that are based on iterating the guessed object between the object plane and the Fourier plane while utilizing prior knowledge about the sample to limit the solution space. These algorithms include ptychography[27, 4] as well as non-scanning CDI methods such as the error reduction algorithm [28, 29, 30, 31]. All these algorithms rely on the information in the measured diffraction pattern to converge to the correct solution. In the following, we show how the available spectrum information in the Fourier domain is redistributed to fill out the missing section of the diffraction pattern.

We demonstrated that the measured diffraction data contains data redundancies. If the size of the beam stop is smaller than the largest angle of illumination, the missing information will be available at other locations. This redundancy enables the recovery of the missing frequencies. The iterative algorithm and knowledge of the illumination function are crucial to this action. We won't go into detail about how a phase retrieval technique operates, as this topic is outside the focus of this study. Interested reader can refer to [43, 44].

Eq.4 describes the diffraction data of a band-limited object $o(x)$ illuminated by the probe $p(x)$ and recorded by the camera.

$$\begin{aligned} I(u) =& |FT[o(x)\ p(x)]|^2 \\ =& |FT[o(x)] * FT[p(x)]|^2 \\ =& |O(u) * (\delta(u-\alpha) + \delta(u+\alpha))|^2 \\ =& |O(u-\alpha) + O(u+\alpha)|^2 \end{aligned} \tag{4}$$

We highlight the fact that there are two locations where the object spectrum is encoded. If the camera is blocked in such a way that the spectrum at location $(u-\alpha)$ is untouched but the information at location $(u+\alpha)$ is lost, The I(u) becomes:

$$I(u) = |O(u-\alpha)|^2 \tag{5}$$

Algorithm 1 describes the ePIE algorithm adapted for pixel masking method and without the update step for probe function. For the sake of simplicity we assume the complete knowledge of the probe and assume only one measured diffraction pattern (J=1). The reconstruction procedure starts by propagating an estimate of the exit wave, constructed by multiplying a random object and the probe function shifted by X_j, to the Fourier domain. There, we enforce the Fourier constraint

Algorithm 1 ePIE algorithm assuming full knowledge of the illumination

while $k = 0, .., \text{maxit}$ **do**
  for all $j = 1, .., J$ **do**
    $\psi_j^k(x) = o^k(x)\ p(x - X_j)$
    $\Psi_j^{k+1}(u) = \mathbf{FFT}[\psi_j^k(x)]$
    Fourier constraint:
    if pixel $\notin$ blocked region **then** ▷ Pixel-masking method
      $\Psi_j^{k+1}(u) = \sqrt{I_j}\frac{\Psi_j^{k+1}(u)}{|\Psi_j^{k+1}(u)|}$
    end if
    $\psi_j^{k+1}(x) = \mathbf{iFFT}[\Psi_j^{k+1}(u)]$
    object update:
    $o^{k+1} = o^k + \frac{(\psi^{k+1}(x) - \psi^k(x))p^*(x-X_j)}{|p(x-X_j)|^2_{max}}$
  end for
end while

by replacing the amplitude of $\Psi^{k+1}(u)$ with the amplitude of the measured data from Eq. 5 and keeping the phase. At this step it is essential to use the pixel masking method. This method enforces the valid information while masking the information in the missing region. This way the incorrect information is not enforced.

Next, the updated guess is propagated back to the spatial domain. At each iteration, the object guess is updated with the information from the previous iteration. In the update formula, we enforce the information on the object spectrum, which was previously fed to the algorithm through the Fourier module constraint ($\psi^{k+1}(x) = \text{iFFT}[\sqrt{I(u)}\frac{\psi^{k+1}(u)}{|\psi^{k+1}(u)|}]$).

$$o^{k+1}(x) = o^k(x) + \frac{(\psi^{k+1}(x) - \psi^k(x))p^*}{|p(x)|^2} \tag{6}$$

Then, the updated object guess $o^{k+1}(x)$ is multiplied by the probe to form the new exit wave guess and is propagated to the far field. From the convolution theorem, we know that the multiplication of two functions in the spatial domain is equal to the convolution of their spectra in the Fourier domain. Convolving the spectrum of the probe with the spectrum of the object dictates the extent and structure of the

spectrum in the Fourier domain. We observe that if the probe is composed of two plane waves at opposite angles, the exit wave in the Fourier domain becomes:

$$\begin{aligned}\Psi_j^{k+1}(u) =& \text{FFT}(\psi_j^k(x)) \\ =& \text{FFT}(o^{(k)}(x)\ p^k(x)) \\ =& \text{FFT}(o^k(x)) * \text{FFT}(e^{i\alpha x} + e^{-i\alpha x}) \\ =& O^k(u) * (\delta(u-\alpha) + \delta(u+\alpha)) \\ =& O^k(u-\alpha) + O^k(u+\alpha)\end{aligned} \tag{7}$$

This shows that the information about the object is now available at the two locations in the Fourier domain. The measured intensity from Eq. 5 used before to update the spectrum guess was missing the spectrum information in the region $(u+\alpha)$. After an iteration of the reconstruction algorithm, the missing data region at $(u+\alpha)$ is updated with an estimate based on the available spectrum information at $(u-\alpha)$. The redundancy generated by the illumination function allows to block a section of the spectrum without losing the complete diffraction spectrum information. Whereas knowledge of probe instructed the reconstruction algorithm to distribute the available information also to the missing data region $(u+\alpha)$

What we showed here is a special case with only two plane waves illuminating the object and with complete knowledge of the illumination function. The concept, however, can be extended to a finite NA illumination. A finite NA illumination is composed of infinite number of plane waves with angles ranging between $[-\theta, +\theta]$, which increases the frequency of encoding the object's spectrum. As long as the extent of the missing information is less than distance between the most oblique plane waves, the iterative algorithm can recover the information in the missing region. It was previously empirically demonstrated in [23] that as long as the beam stop is smaller than the size of the projection of the probe on the detector, the lost frequencies can be recovered. Later, the theoretical and experimental results from [24] solidified the significant reliance of CDI algorithms on the dimensions of the probe for the task of retrieving the missing information. They showed that the recovery of missing saturated pixel data in the central region of the diffraction patterns is possible only if the extent of saturated pixels is less than the extent of the probe in the Fourier plan.

The problem of recovering the missing signal from known information is a well researched topic in the signal processing community [34, 35]. The procedure of illuminating an object with a probe can find an analogy in modulating a signal with a carrier wave where the signal corresponds to the object and the carrier wave is the

illumination function. This results in the replication of the spectrum of the signal according to the frequency of the carrier wave [36]. By demodulating the signal at the receiver, the original signal can be recovered. The problem of the recovery of a signal in the presence of missing data points is investigated by [36, 37] where it is shown that when a band-limited signal is sampled at a frequency higher than the Nyquist sampling rate, it is possible to recover the missing sample points using an iterative procedure similar to the one we described here.

3. Results and discussions

3.1. Experimental results

For the experimental demonstration, we used RESCAN, an actinic EUV lensless microscope operating at the XIL-II beamline of the Swiss Light Source (see Fig. 4 (left)) [38, 39, 40]. The EUV beam with a wavelength of $\lambda = 13.5$ nm is focused on the sample by a multilayer-coated toroidal mirror (M_1). A flat mirror (M_2) directs the light towards the sample at an incidence angle of 6 degrees. For this experiment, we used a sample constituted by a silicon wafer coated with a Mo/Si multilayer. The multilayer is designed to reflect EUV light at an angle of incidence between 0 and 12 degrees. The multilayer is covered with an absorber layer of hydrogen silsesquioxane (HSQ) with a thickness of 140 nm, patterned with e-beam lithography [39, 40]. The pattern on the sample includes a Siemens star with 15 fans (see Fig. 5). Pytchography assumes thin object interactions for the calculation of the exit wave. Our experiments use low NA illumination, and therefore, the shift variance still holds even though that the object thickness is almost ten times the size of the wavelength.

We scanned the sample over a circular area with a diameter of 6 µm, centered on the Siemens star. The scan step size was 1 µm to ensure a probe overlap of 68% [41]. A detector with 2048×2048 pixels and a pixel size of 13.5 µm (CCD, Princeton Instruments MTE-2) collects the diffraction patterns at a distance of 62 mm from the sample, which corresponds to the detection NA of 0.22. The collected diffraction intensities are centered and a background image is subtracted from the diffraction set. This pre-processing step reduces the image size to 1800×1800 pixels. Afterward, we use a ptychography algorithm based on the difference map method [4, 42] to reconstruct the complex amplitude of the object and the illumination probe. We compare the reconstructed image with a reference image (die-to-database) to inspect the quality of the reconstruction [39]. The reference image is computed from the sample's fabrication pattern. The pattern is passed through an imaging system, illuminated by a plane wave of the same wavelength, and detected using

a detector with NA identical to the experimental setup. The reconstructed image and the reference were registered and normalized. To measure the accuracy of the reconstructed image, we used an image fidelity metric defined as:

$$E = \frac{\sum |I_{\text{ref}} - I_{\text{rec}}|}{N} \tag{8}$$

where I_{ref} is the reference image intensity, I_{rec} is the reconstructed image intensity and N is number of pixels of the image. The experimental setup does not have a

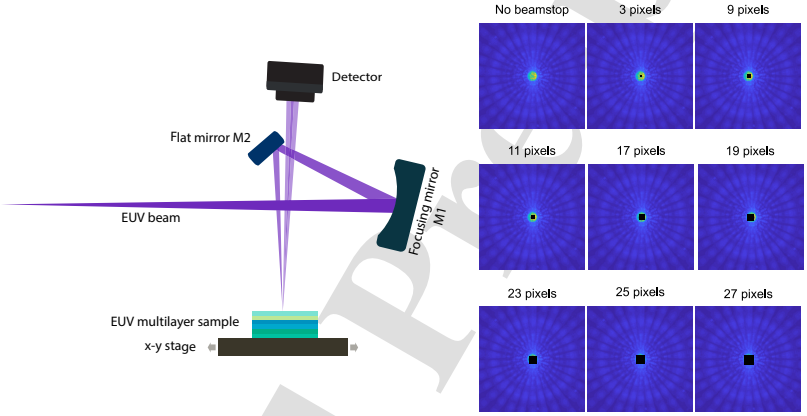

Figure 4: EUV experimental setup at XIL beamline (left). The beam from XIL beamline reaches the focusing mirror M_1. After reflecting from the flat mirror M_2, it hits the object at an angle of 6 degrees. Part of the diffracted light is collected by the detector. The images on the right depict the diffraction intensity images collected with the RESCAN microscope. We applied an artificial beam stop blocking the central part of the diffraction patterns.

physical beam stop. We simulated the effect of a beam stop by setting the pixels corresponding to the beam stop area to zero, as shown in Fig. 4. We then used the pixel masking method to enable the algorithm to converge to the correct solution. This approach differs from an actual beam stop as we don't consider the diffraction effect caused by the beam stop edges, which is a negligible effect in most cases. The illumination NA in the RESCAN setup is 0.0026 which corresponds to a cone with a diameter of 23 pixels on the detector plane. We simulated beam stops with a diameter between 0 and 27 pixels, equivalent to blocking diffraction angles corresponding to NA values from 0 to 0.0029. The reconstructed images are shown in Fig. 5. We observe a drop in the contrast for beam stop diameters larger

than 23 pixels. Fig. 6 depicts the reconstructed images using simulation data, in which we observe a similar trend. These images were used in Fig. 7(a) to confirm the critical size of the beam stop. In Fig. 7(a), we verify that the reconstruction

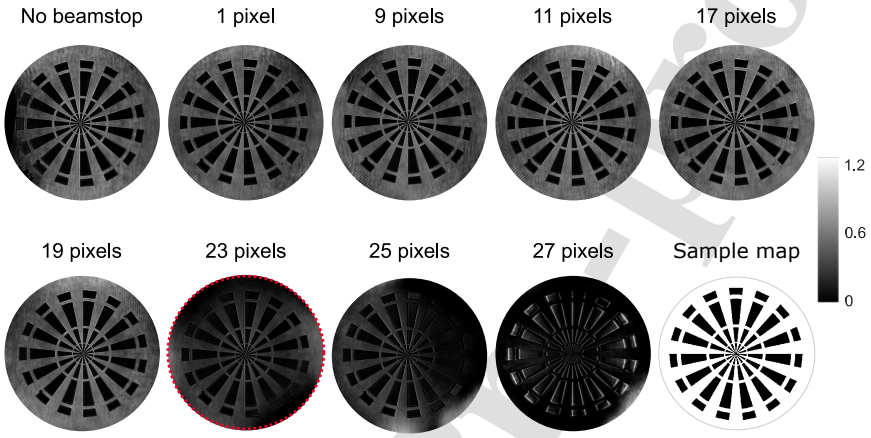

Figure 5: Reconstructed intensities corresponding to different beam stop sizes. Each pixel of the detector corresponds to 13.5 µm. The reconstructed intensity circled in red corresponds to the case where the beam stop size is almost equal to the cone defined by the illumination NA.

error of the simulated and the experimental data have a similar turning point at a beam stop diameter of 23 pixels. The difference in the scale of the error is due to noise and uncertainty in the object's positioning. Before reaching the NA limit, the remaining replicas of the spectrum enable the reconstruction algorithm to converge to the correct solution. Therefore, we get a constant low error. But as soon as the last replica of the object's spectrum is obscured, the error abruptly increases.

Fig. 7(b), shows the relation between contrast, spatial frequency and the size of the beam stop. The modulation transfer function (MTF), specifies how the imaging system affects the different spatial frequencies of the object. Here, the MTF plots represent the contrast of the reconstructed pattern as a function of the spatial frequency. As the size of the beam stop exceeds 23 pixels, corresponding to the NA_{ill}, the contrast drastically drops (the two lower lines). The highest contrast loss happens at the lower frequencies which are now completely obscured by the beam stop. We see that for both larger beam stop sizes of 25 pixels and 27 pixels, the most susceptible spatial range stays consistent.

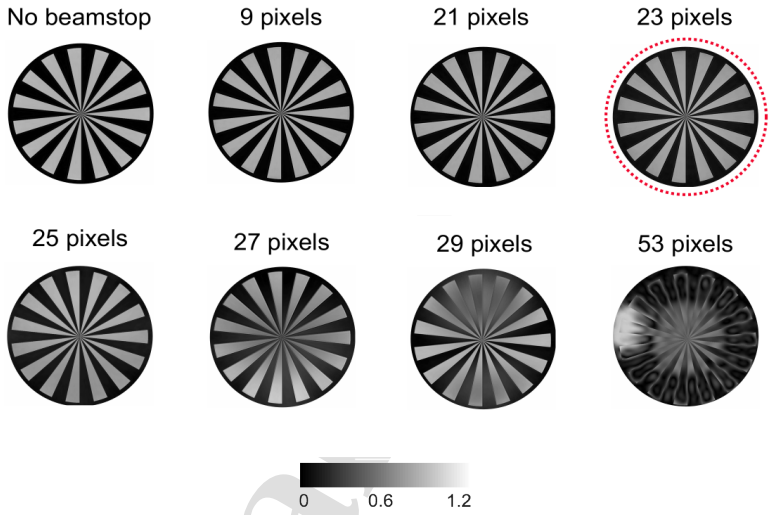

Figure 6: Reconstructed images of simulated data with illumination NA of 0.0026 (same as the experimental setup). We can visually see the contrast drop and presence of artifacts as the beam stop size becomes larger than the size of the illumination NA. The reconstruction marked by the red dotted circle corresponds to the case where the beam stop size is closest to the illumination NA.

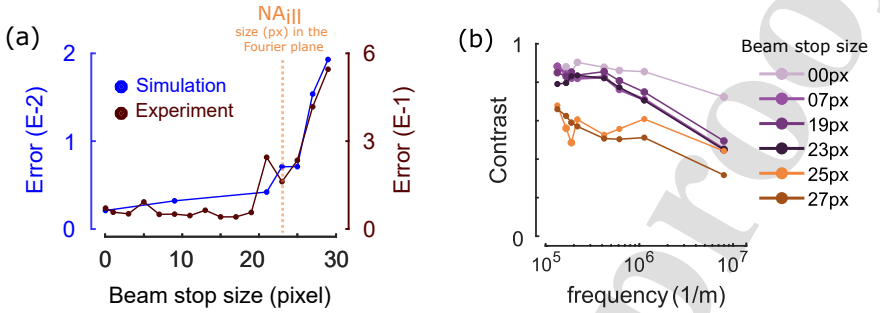

Figure 7: Analysis of data corresponding to NA_{ill} of 0.0026. (a) Comparison of experimental (burgundy) and simulation (blue) MSE plots. In both cases, the reconstruction quality starts degrading when the beam stop size is larger than NA_{ill}. (b) The image contrast drops for beam stop sizes above the illumination NA. The lower spatial frequencies suffer the most as their spectrum replicas are not present anymore.

3.2. Simulations for extended illumination NA

The illumination NA of RESCAN is limited to a very narrow range. Therefore, in the previous section, the experimental and simulation results are only for a single illumination NA. In this section, we simulate a broader range of NA_{ill} to verify the frequency replication theory. We use the same physical parameters in the simulations as our EUV experimental setup, keeping the wavelength, propagation distance, and CCD properties the same. We change the focusing mirror's focal length and the distance from the focus to produce ptychographic data sets with different NA_{ill} values but constant illumination size on the object. The simulated diffraction pattern intensities on the detector plane are obscured by rectangular beam stops of increasing size. The data in these regions was set to zero. The obscured diffraction patterns are reconstructed using the same reconstruction algorithm used for the experimental data presented in Section 3.1.

Fig. 8 depicts the evolution of error values for several reconstructions with different illumination NAs. The range of the illumination NAs is between 0.0026 and 0.1. The dashed line marks the point where the beam stop size equals the size of the illumination NA on the detector. Before this limit, an increase in the size of the beam stop does not affect the reconstruction process. When the size of the beam stop becomes larger than NA_{ill}, the error values for all the plots increase independently of their NA_{ill}. This demonstrates that in order to preserve the quality of the reconstruction, the maximum size of a beam stop should be less than the illumination NA.

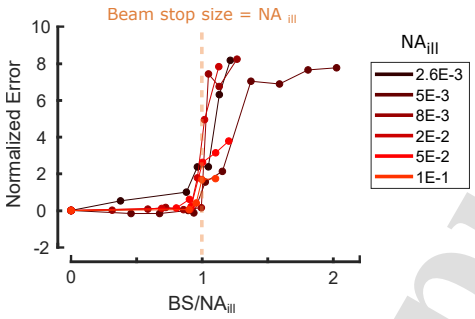

Figure 8: Mean square error analysis of reconstructed images as a function of the beam stop (BS) size normalized to the size of the illumination NA. We observe that regardless of the illumination NA value, the error abruptly rises as we surpass the size of illumination NA in the Fourier domain. The error values are percentage errors normalized to the reconstructed image without any obscuration.

4. Conclusion

CDI methods rely on the diffraction amplitude collected by a 2D pixel detector to reconstruct the image of the sample under investigation. If certain regions of the recorded diffraction spectra are missing because of the presence of a beam stop or contain unreliable data because of the limitations of the detector, the corresponding pixels are ignored, and their value is not used when the Fourier amplitude constraint is enforced. This is a common approach known as the pixel masking method.

We investigated the limits of the pixel masking method with experiments, simulations, and theoretical analysis. We performed simulations of ptychography datasets with different beam stop sizes. We defined an error metric to study the quality of the reconstruction and observed a sharp deterioration of the reconstruction quality as soon as the beam stop size exceeds the size of the probe projection in the Fourier plane. This result was confirmed by reconstructing the experimental data with different beam stop sizes. In this case, we evaluated the reconstructions using the same error metric for the image quality and measured the modulation transfer function as a function of the beam stop size. We observed that a sharp drop in contrast happens when the beam stop size is larger than the size of illumination NA on the detector. This result is in agreement with previous experimental works [25, 26, 23, 24]. Specifically, there is a contrast drop for the lower frequencies, which cannot be recovered anymore. We can, therefore, conclude that the size of the illumination NA is a critical factor for the reconstruction quality in the case

of missing information at the detector plane. A simple theoretical explanation is given for the behaviour of the reconstruction algorithm in the presence of a beam stop. We traced two plane waves in the illumination function to show that as long as the diffraction frequencies lost because of the beam stop (or the defective detector areas) are encoded somewhere else in the recorded diffraction patterns, the iterative CDI algorithm can recover the image of the sample correctly which is the same conclusion obtained in [24]. By analytically tracing the steps of the reconstruction algorithm, we were able to show that the recovery of the missing data is due to the extended size of the high intensity region of the illumination Fourier spectrum.

In this study, we discussed the impact of increasing the NA of the illumination system as well as the implications of information redundancy on the detector. The presence of redundancy facilitates the use of larger beam stops. However, the goal to achieve the maximum attainable illumination NA is not a practical approach. Increasing the NA results in a reduction in the intensity of the diffraction pattern. Additionally, the feasibility of achieving a high illumination NA in extreme ultraviolet (EUV) is restricted by the challenges posed by the experimental setup. Furthermore, the shift-invariance constraint of ptychography imposes limitations on the maximum extent of the illumination NA. The findings presented in this paper are most effectively applied towards determining the optimal size of a beam stop within a given experimental configuration through the identification of the maximum tolerable frequency loss. The perspective provided in this research can be used to choose the proper size for the beam stop depending on the illumination NA for a ptychography or CDI setup, with particular regard to EUV systems. The analysis of the reconstructed images from simulation data supports the idea of the impact of the illumination NA on the recovery of missing frequencies. Finally, we analyzed the effect of the beam stop on the MTF of the reconstructed image to optimize the experimental setup, including the beam stop size and the tiling of the detector.

Funding

Part of this research was performed at Swiss Light Source, Paul Scherrer Institut. The authors thank the Swiss National Science Foundation for financial support (SNF Grant Number: 200021- 172768).

Acknowledgments

We wish to acknowledge the contribution of Dimitrios Kazazis and the technical support team at PSI, Michaela Vockenhuber, Markus Kropf and Josè Gabadinho.

We extend special thanks to Prof. Dr. Gabriel Aeppli for invaluable discussions. Disclosures The authors declare no conflicts of interest

References

[1] Hegerl, Reiner, and W. Hoppe. "Dynamische theorie der kristallstrukturanalyse durch elektronenbeugung im inhomogenen primärstrahlwellenfeld." Berichte der Bunsengesellschaft für physikalische Chemie 74.11 (1970): 1148-1154.

[2] Miao, Jianwei, et al. "Extending the methodology of X-ray crystallography to allow imaging of micrometre-sized non-crystalline specimens." Nature 400.6742 (1999): 342-344.

[3] Nellist, P. D., B. C. McCallum, and John M. Rodenburg. "Resolution beyond the'information limit'in transmission electron microscopy." Nature 374.6523 (1995): 630-632.

[4] Thibault, Pierre, et al. "High-resolution scanning x-ray diffraction microscopy." Science 321.5887 (2008): 379-382.

[5] Rodenburg, John M., and Helen ML Faulkner. "A phase retrieval algorithm for shifting illumination." Applied physics letters 85.20 (2004): 4795-4797.

[6] Mochi, Iacopo, et al. "Experimental evaluation of the impact of carbon nanotube EUV pellicles on reticle imaging." Journal of Micro/Nanolithography, MEMS, and MOEMS 18.1 (2019): 014002.

[7] Giewekemeyer, Klaus, et al. "Quantitative biological imaging by ptychographic x-ray diffraction microscopy." Proceedings of the National Academy of Sciences 107.2 (2010): 529-534.

[8] Agard, David A., Yasushi Hiraoka, and John W. Sedat. "Three-dimensional microscopy: image processing for high resolution subcellular imaging." New methods in microscopy and low light imaging. Vol. 1161. SPIE, 1989.

[9] Holler, Mirko, et al. "High-resolution non-destructive three-dimensional imaging of integrated circuits." Nature 543.7645 (2017): 402-406.

[10] Attwood, David. Soft x-rays and extreme ultraviolet radiation: principles and applications. Cambridge university press, 2000.

[11] Mochi, Iacopo, et al. ”Resolution enhancement for lensless mask metrology with RESCAN.” International Conference on Extreme Ultraviolet Lithography 2019. Vol. 11147. SPIE, 2019.

[12] O’Leary, Colum M., et al. ”Contrast transfer and noise considerations in focused-probe electron ptychography.” Ultramicroscopy 221 (2021): 113189.

[13] Chang, Huibin, et al. ”Advanced denoising for X-ray ptychography.” Optics express 27.8 (2019): 10395-10418.

[14] Zuo, J. M., et al. ”Atomic resolution imaging of a carbon nanotube from diffraction intensities.” Science 300.5624 (2003): 1419-1421.

[15] Miao, Jianwei, et al. ”Phase retrieval of diffraction patterns from noncrystalline samples using the oversampling method.” Physical Review B 67.17 (2003): 174104.

[16] Wilke, R. N., M. Vassholz, and T. Salditt. ”Semi-transparent central stop in high-resolution X-ray ptychography using Kirkpatrick–Baez focusing.” Acta Crystallographica Section A: Foundations of Crystallography 69.5 (2013): 490-497.

[17] He, Kuan, Manoj Kumar Sharma, and Oliver Cossairt. ”High dynamic range coherent imaging using compressed sensing.” Optics Express 23.24 (2015): 30904-30916.

[18] Marchesini, S., et al. ”Coherent X-ray diffractive imaging: applications and limitations.” Optics Express 11.19 (2003): 2344-2353.

[19] Guizar-Sicairos, Manuel, and James R. Fienup. ”Phase retrieval with transverse translation diversity: a nonlinear optimization approach.” Optics express 16.10 (2008): 7264-7278.

[20] Rose, Max, et al. ”Quantitative ptychographic bio-imaging in the water window.” Optics express 26.2 (2018): 1237-1254.

[21] Dierolf, Martin Johannes. Ptychographic X-ray microscopy and Tomography. Diss. Technische Universität München, 2015.

[22] Enders, B., and P. Thibault. "A computational framework for ptychographic reconstructions." Proceedings of the Royal Society A: Mathematical, Physical and Engineering Sciences 472.2196 (2016): 20160640.

[23] Miao, Jianwei, et al. "Quantitative image reconstruction of GaN quantum dots from oversampled diffraction intensities alone." Physical review letters 95.8 (2005): 085503.

[24] Pan, XingChen, et al. "Ptychographical imaging with partially saturated diffraction patterns." Journal of Modern Optics 62.15 (2015): 1270-1277.

[25] Liu, Haigang, et al. "Effects of missing low-frequency information on ptychographic and plane-wave coherent diffraction imaging." Applied Optics 52.11 (2013): 2416-2427.

[26] Latychevskaia, Tatiana. "Reconstruction of missing information in diffraction patterns and holograms by iterative phase retrieval." Optics Communications 452 (2019): 56-67.

[27] Rodenburg, John M., and Helen ML Faulkner. "A phase retrieval algorithm for shifting illumination." Applied physics letters 85.20 (2004): 4795-4797.

[28] Fienup, James R. "Reconstruction of an object from the modulus of its Fourier transform." Optics letters 3.1 (1978): 27-29.

[29] Fienup, James R. "Phase retrieval algorithms: a comparison." Applied optics 21.15 (1982): 2758-2769.

[30] Marchesini, Stefano. "Invited article: A unified evaluation of iterative projection algorithms for phase retrieval." Review of scientific instruments 78.1 (2007): 011301.

[31] Daurer, Benedikt J. Algorithms for Coherent Diffractive Imaging with X-ray Lasers. Diss. Acta Universitatis Upsaliensis, 2017.

[32] Chapman, Henry N., et al. "High-resolution ab initio three-dimensional x-ray diffraction microscopy." JOSA A 23.5 (2006): 1179-1200.

[33] Giewekemeyer, Klaus, et al. "High-dynamic-range coherent diffractive imaging: ptychography using the mixed-mode pixel array detector." Journal of synchrotron radiation 21.5 (2014): 1167-1174.

[34] Donoho, David L., and Philip B. Stark. "Uncertainty principles and signal recovery." SIAM Journal on Applied Mathematics 49.3 (1989): 906-931.

[35] Needell, Deanna, and Roman Vershynin. "Signal recovery from incomplete and inaccurate measurements via regularized orthogonal matching pursuit." IEEE Journal of selected topics in signal processing 4.2 (2010): 310-316.

[36] Shynk, John J. Mathematical foundations for linear circuits and systems in engineering. John Wiley & Sons, 2016.

[37] Marks, Robert J. "Multidimensional-signal sample dependency at Nyquist densities." JOSA A 3.2 (1986): 268-273.

[38] Mochi, Iacopo, et al. "Resolution enhancement for lensless mask metrology with RESCAN." International Conference on Extreme Ultraviolet Lithography 2019. Vol. 11147. SPIE, 2019.

[39] Mochi, Iacopo, et al. "Actinic inspection of EUV reticles with arbitrary pattern design." International Conference on Extreme Ultraviolet Lithography 2017. Vol. 10450. SPIE, 2017.

[40] Mochi, Iacopo, et al. "Through-pellicle inspection of EUV masks." Extreme Ultraviolet (EUV) Lithography IX. Vol. 10583. SPIE, 2018.

[41] Bunk, Oliver, et al. "Influence of the overlap parameter on the convergence of the ptychographical iterative engine." Ultramicroscopy 108.5 (2008): 481-487.

[42] Maiden, Andrew M., and John M. Rodenburg. "An improved ptychographical phase retrieval algorithm for diffractive imaging." Ultramicroscopy 109.10 (2009): 1256-1262.

[43] Fienup, James R. "Phase retrieval algorithms: a personal tour." Applied optics 52.1 (2013): 45-56.

[44] Fienup, James R. "Phase retrieval algorithms: a comparison." Applied optics 21.15 (1982): 2758-2769.

- Ptychography a lensless imaging technique used in extreme ultraviolet and X-ray imaging retrieves a sample's complex amplitude
- Pixel masking method solves data loss problem due to oversaturation or detector pixel defects using iterative algorithm
- Verify the limits of the pixel masking method to recover the missing information due to a beam stop in a EUV setup
- Quantify the quality of reconstructed image at the presence of a beam stop based on simulation and EUV experimental data to identify the vulnerable spatial frequencies.